Mineralogy of Occator Crater on Ceres

A. Raponi[a], M.C. De Sanctis[a], F.G. Carrozzo[a], M. Ciarniello[a], J. C. Castillo-Rogez[b], E. Ammannito[c], A. Frigeri[a], A. Longobardo[a], E. Palomba[a], F. Tosi[a], F. Zambon[a], C.A. Raymond[b], C.T. Russell[d].

[a] INAF-IAPS Istituto di Astrofisica e Planetologia Spaziali, Via del Fosso del Cavaliere, 100, I-00133 Rome, Italy;
[b] NASA/Jet Propulsion Laboratory, California Institute of Technology, 4800 Oak Grove Drive, Pasadena, CA 91109, United States;
[c] Italian Space Agency (ASI), Via del Politecnico snc, I-00133 Rome, Italy;
[d] Institute of Geophysics and Planetary Physics, University of California at Los Angeles, 3845 Slichter Hall, 603 Charles E. Young Drive, East, Los Angeles, CA 90095-1567, United States.

Abstract. Occator Crater on dwarf planet Ceres hosts the so-called faculae, several areas with material 5 to 10 times the albedo of the average Ceres surface: Cerealia Facula, the brightest and larger, and several smaller faculae, Vinalia Faculae, located on the crater floor. The mineralogy of the whole crater is analyzed in this work. Spectral analysis is performed from data of the VIR instrument onboard the Dawn spacecraft. We analyze spectral parameters of all main absorption bands, photometry, and continuum slope. Because most of the absorption features are located in a spectral range affected by thermal emission, we developed a procedure for thermal removal. Moreover, quantitative modeling of the measured spectra is performed with a radiative transfer model in order to retrieve abundance and grain size of the identified minerals. Unlike the average Ceres surface that contains Mg-Ca-carbonate, Mg-phyllosilicates, NH_4-phyllosilicats, the faculae contain Na-carbonate, Al-phyllosilicates, and NH_4-chloride. Significant differences in the concentrations of these minerals between Vinalia and Cerealia Faculae have been analyzed. Moreover, heterogeneities are also derived within Cerealia Facula that might reflect different deposition events of bright material. An interesting contrast in grain size is found between the center of the faculae (10-60 μm) and the crater floor/peripheral part of the faculae (100-130 μm), pointing to different cooling time of the grains, respectively faster and slower, and so to different time of formation with respect the source of heat released by the impact. This would imply more recent faculae formation than the crater impact event. For some ejecta we derived larger concentration of minerals producing the absorption bands, and smaller grains with respect the surrounding terrain. This should be related to heterogeneity of the material preexistent to the impact event.

1. Introduction

NASA's Dawn spacecraft (Russell and Raymond, 2011) arrived at dwarf planet Ceres on March 6, 2015, with its scientific payload: the Visible and near-InfraRed imaging spectrometer (VIR) (De Sanctis et al., 2011), the Gamma Ray and Neutron Detector (GRaND) (Prettyman et al., 2011), and the Framing Camera (FC) (Sierks et al., 2011), along with the radio science package (Konopliv et al., 2011).

Ceres' surface shows ubiquitous absorption bands at 2.7 μm (OH stretching) and 3.1 μm related to Mg-phyllosilicates and NH_4-phyllosilicates, respectively (De Sanctis et al., 2015; Ammannito et al., 2016). The thermally-corrected reflectance spectrum of Ceres shows several distinct absorption bands at 3.3-3.5, and 3.95 μm, due to the presence of Mg-carbonates (De Sanctis et al., 2015).

Although the spectral properties of Ceres' surface are quite uniform, there are several peculiar areas with brighter material where significant differences in spectral parameters have been detected, such as slopes, albedo, band depths and band center of specific spectral features (Palomba et al. this issue, Stein et al. this issue). The features that stand out from the surrounding terrains are the bright areas, called "Ceralia and Vinalia Faculae," in the 92-km-diameter Occator crater (15.8-24.9 °N and 234.3-244.7 °E). Their albedo is 5-10 times higher than the average surface (Longobardo et al., this issue, Li et al. 2016, Ciarniello et al. 2017, Schroder et al. 2017, Longobardo et al. submitted).

Bright material in the faculae has many spectral differences with respect the crater floor. The OH feature in these faculae is shifted from 2.72 to 2.76 μm, indicating the possible presence of Al-phyllosilicates. A very complex spectral feature is present at 3.0 – 3.6 μm, with the superposition of a band at 3.1 μm, two absorption bands at 3.2 and 3.28 μm, and the absorption band of carbonate at 3.4 and 3.5 μm. The origin of the absorption bands at 3.1, 3.2 and 3.28 is still unknown. Moreover a clear and deep absorption at 4 μm indicate the presence of Na-carbonates (De Sanctis et al., 2016).

Occator crater (Figure 1) contains different geological units: smooth and knobby lobate materials, hummocky crater floor material, and the faculae, respectively from the older to the more recent as discussed by Scully et al. (this issue). Dawn's Framing Camera has observed the Cerealia Facula at high spatial resolution (35 m/pix) revealing that it is located in a ~9 km wide and ~700 m deep pit. A dome in the center of the pit rises 0.4 km above the surrounding terrain (Nathues et al., 2017). The faculae are associated with fractures in Occator's floor (Buczkowski et al. 2016). The formation process proposed for the faculae includes impact-induced heating and the subsequent upwelling of volatile-rich materials, possibly rising to the surface along impact-induced fractures from subsurface brines' reservoir (Scully et al. this issue, Stein et al. this issue). It has also suggested that the faculae could have deposited from post-impact plumes formed through boiling of subsurface solutions (Zolotov, 2016).

Here, we use data returned by the VIR instrument in order to study the mineralogical composition of the Occator Crater region. We start the analysis subtracting the thermal emission from the spectra with a procedure described in Section 3. Then we analyze absolute signal level, spectral slope, and the spectral parameter of the main absorption bands, as described in Section 4. We also retrieve the abundances and the grain size of the main minerals identified as component of the Occator surface materials from a quantitative analysis by means of a radiative transfer model. The model and resulting maps are shown in Section 5. The results are discussed in Section 6 in the general context of the Occator crater evolution.

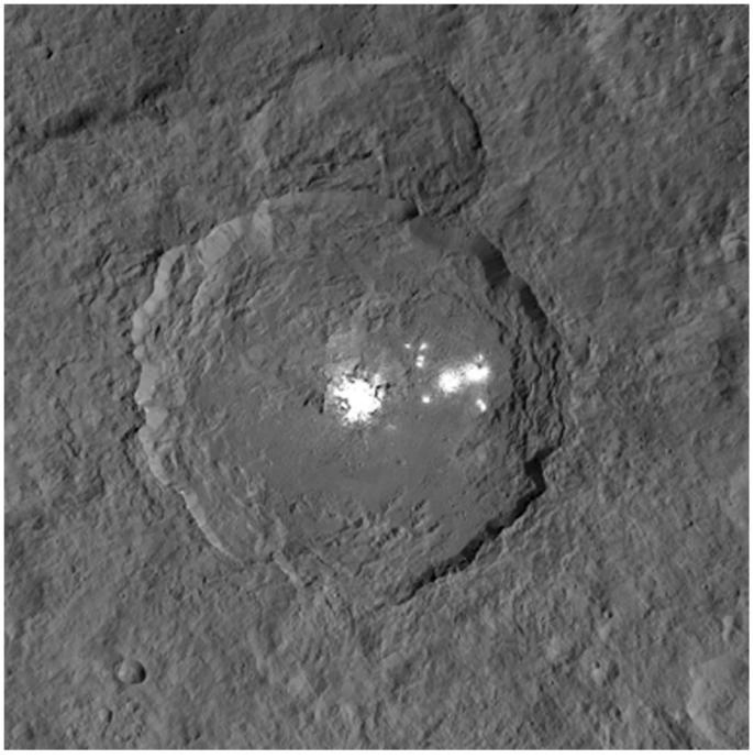

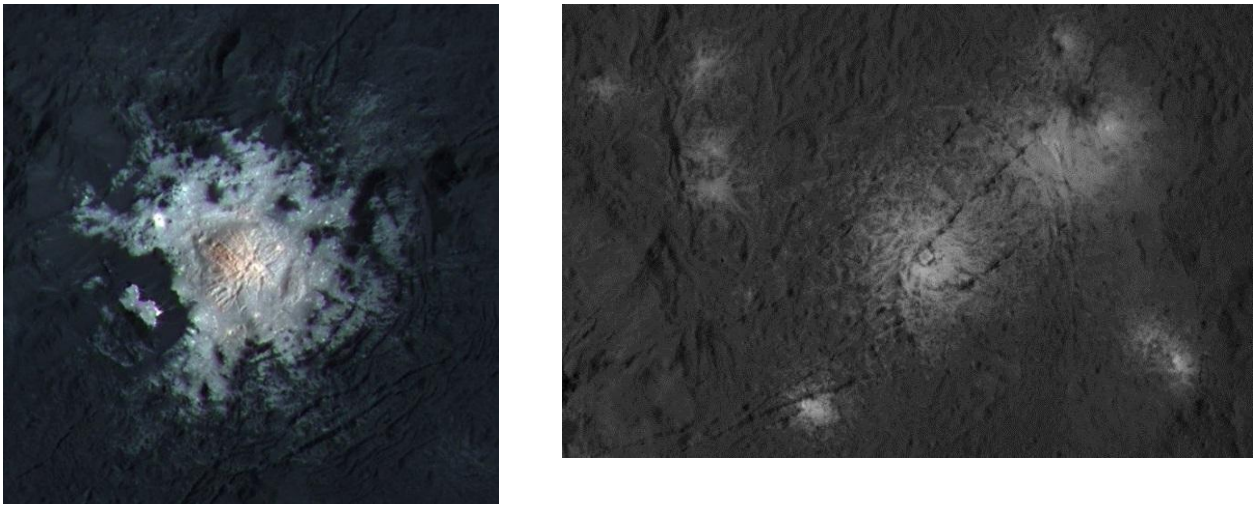

Figure 1. Upper panel. Framing Camera mosaic (35 m/pixel) obtained with clear filter during the Low Altitude Mapping Orbit (LAMO) (Roatsch et al. 2016). Lower left panel: Cerealia Facula obtained by combining framing camera images acquired during LAMO phase with three images using spectral filters centered at 438, 550 and 965 nanometers, during HAMO phase. Lower right panel: Vinalia Faculae acquired by the framing camera during LAMO phase.

2. Data Analysis Description

The present work is built on the dataset acquired by VIR-IR mapping spectrometer. Images provided by the Dawn Framing Camera are also used for context, and morphological analysis.

VIR is an imaging spectrometer operating in two channels: the visible channel, ranging between 0.25-1.05 μm, and the infrared channel, between 1.0-5.1 μm. VIR is capable of high spatial (IFOV= 250 μrad/pixel, FOV= 64 × 64 mrad) and spectral ($\Delta\lambda$VIS = 1.8 nm/band; $\Delta\lambda$IR = 9.8 nm/band) resolution performance, allowing for the identification of spectral features in order to derive the composition and structure of the surface, and its thermal emission.

VIR acquired data of Ceres during all of the mission phases: Survey (spacecraft altitude 4350 km), High Altitude Mapping Orbit (HAMO) (spacecraft altitude 1450 km) and Low Altitude Mapping Orbit (LAMO) (spacecraft altitude 370 km) (Russell and Raymond, 2011). Here, we used HAMO and LAMO datasets with nominal spatial resolutions of 400 m/pix and 100 m/pix, respectively.

The calibrated data (Filacchione and Ammannito, 2014) are cleaned of artifacts with the procedure described in Carrozzo et al. (2016). In order to analyze the spectral signature in the range of wavelengths affected by thermal emission (usually from 3.2 μm longward), we remove thermal emission using the method described in section 3. Photometric effects are corrected for both topographic variations and physical/optical characteristics of the regolith using the Hapke approach (Ciarniello et al., 2016). However, other methods for photometric correction could be applied (Longobardo et al., this issue), yielding similar results.

We selected all spectra whose footprint is located within ~70 km from the crater center in order to account for all the crater floor (radius ~45 km), and the ejecta outside the crater rim. The whole dataset contain ~$3 \cdot 10^5$ spectra of the IR channel. The present work focuses on the spectral range 1.1 - 4.2 μm, which accounts for 328 out of 432 spectels of the whole range.

3. Thermal Emission Removal

The observed spectra of Ceres' surface are affected by thermal emission from ~3.2 μm longward. The radiance of the thermal emission hides the absorption bands and prevents a comparison with laboratory data. We implemented a proper algorithm in order to remove the thermal emission while preserving the spectral features present in the spectra. The total radiance is modeled as the sum of the solar radiance reflected by the surface and the thermal emission of the surface itself, as follows:

- The model of the solar reflected radiance is produced by a model of reflectance of the surface, multiplied by the solar irradiance at Ceres' heliocentric distance. To be consistent

with the spectral modeling discussed in Section 5 we used the same reflectance model to estimate the reflectance level in the thermal emission range.

- The Planck function is summed up to this model in order to fit the total radiance level. Free parameters of the Planck function are temperature and emissivity. Their retrieved values are not discussed in the present work.
- Once the Planck function has been derived, we subtract it from the total measured radiance, and we divide the result by the solar irradiance to obtain the reflectance in the whole range.

Examples of the resulting spectra after thermal emission removal are shown in figure 2.

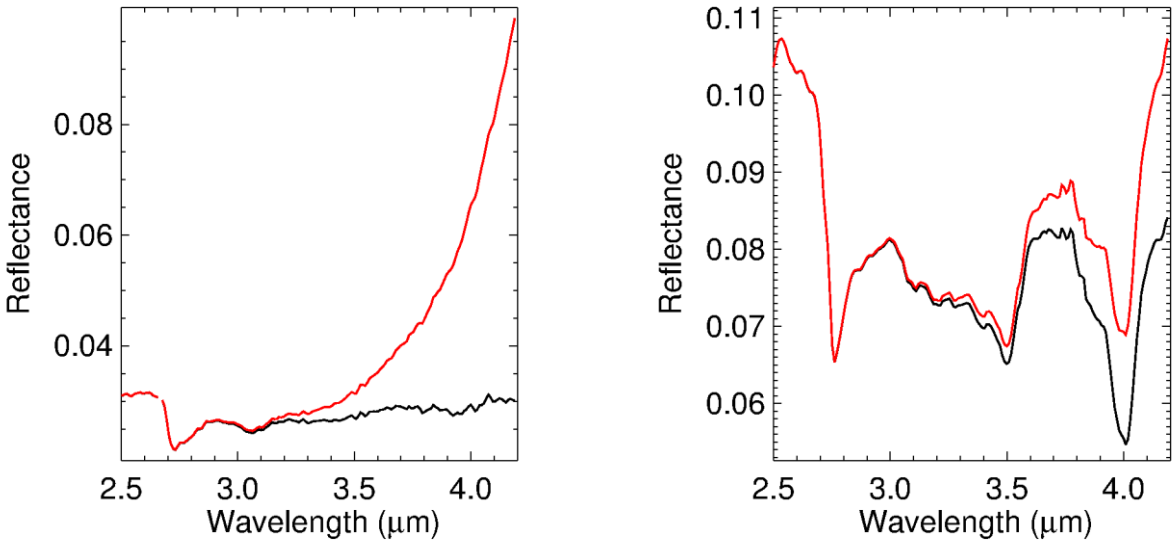

Figure 2. Left panel: thermal emission removal of a typical spectrum of the average surface of Ceres, taken at the rim of Occator crater. Red and black lines are respectively the reflectance spectra before and after thermal emission removal. Right panel: same as left panel for a spectrum acquired at the Vinalia Faculae.

The reflectance continuum in the thermal emission range, after removal of the Planck function, could be over or underestimated depending on the reflectance model used. However, the measured spectral features are not affected by this uncertainty.

4. Spectral analysis

4.1 Data reduction and methodology

To analyze a large dataset like the one considered in this work, we developed an automatic data process able to return different spectral indicators from Occator crater observations. This algorithm allows mapping the spatial distribution of each spectral indicator across the surface. The spectral parameters chosen for this purpose are defined based on the first analysis of the VIR spectra of the average terrain (De Sanctis et al., 2015), Cerealia and Vinalia Faculae (De Sanctis et al., 2016). The parametres are: photometrically corrected reflectance at 2.0 μm, spectral slope between 1.65 and 2.35 μm normalized to the continuum level, band area and center of phyllosilicate bands at 2.7 and 3.1 μm, band area and center of carbonate at 3.5 and 4.0 μm, band area of ammonium salts at 2.2 μm, band area of an unknown component at 3.2 and 3.28 μm mostly present in correspondence of the faculae.

The band area is defined as:

$$\int_a^b \left[1 - \frac{reflectance(\lambda)}{continuum(\lambda)}\right] d\lambda,$$

where *a* and *b* are the edges of the band. The continuum used to characterize the bands is calculated with a linear fit between *a* and *b*. The band area is expressed in μm units.
The band center is defined as the wavelength corresponding to the minimum of the absorption band after continuum removal.

The main spectral differences between the average floor of the crater and the faculae are reported in Figures 3 and 4.

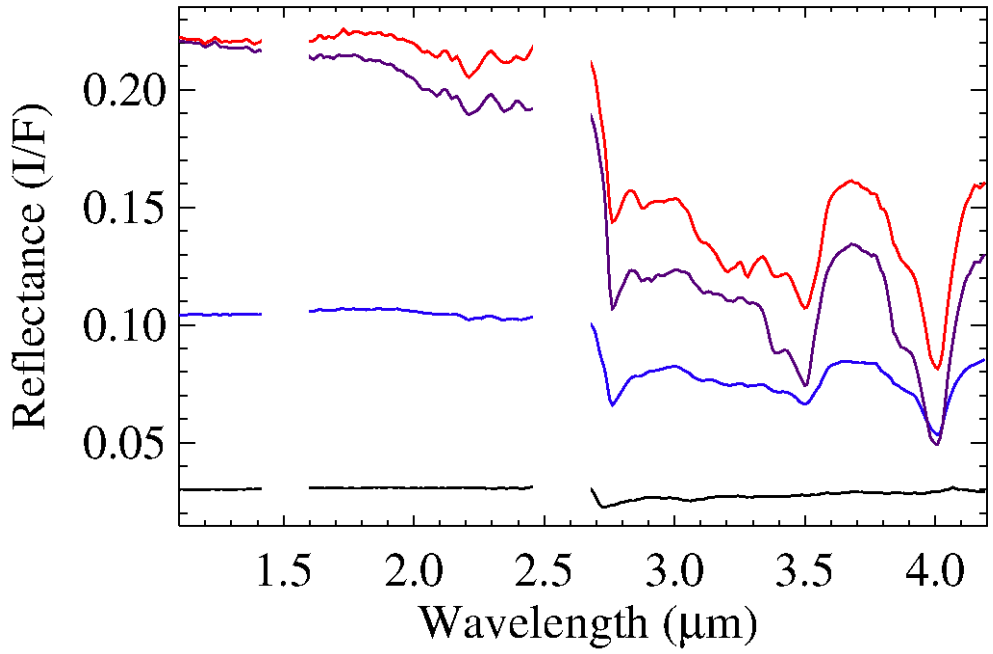

Figure 3. Collected spectra: typical floor spectrum (black line), a Vinalia Facula spectrum (blue line), and two types of Cerealia Facula spectra (red and purple spectrum), which differ in the spectral range 3.2 – 3.4 μm.

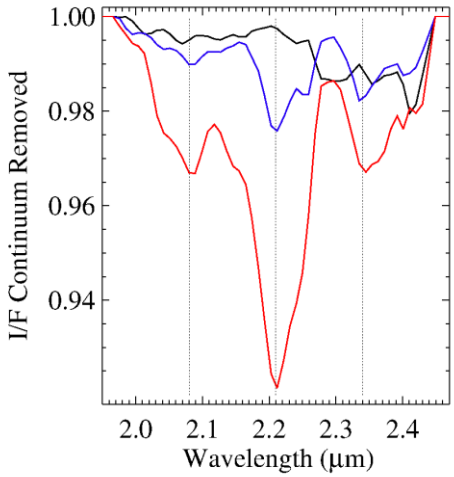

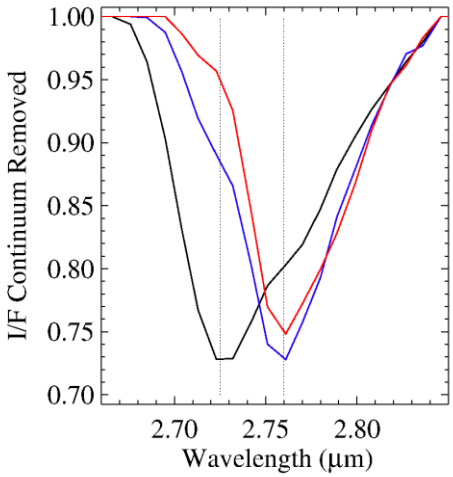

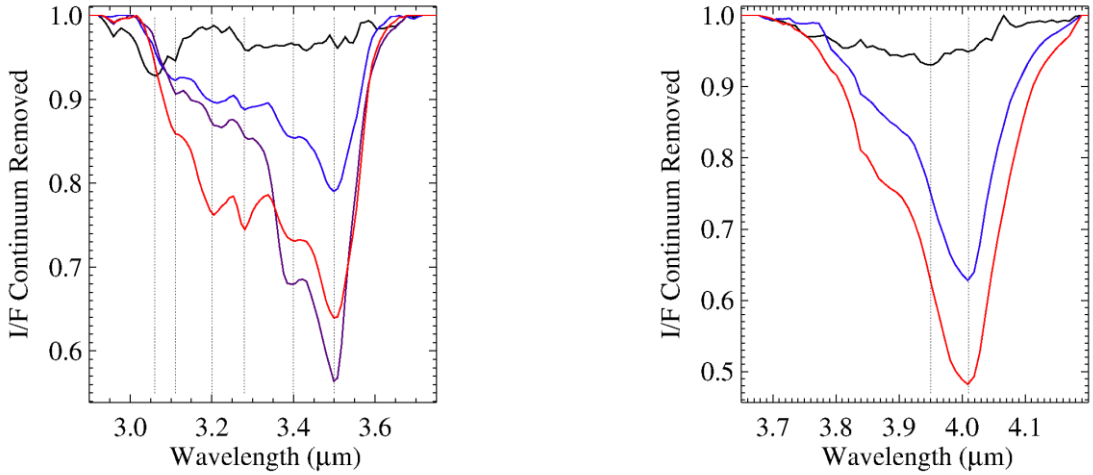

Figure 4. Main spectral difference between a typical floor spectrum (black line), a Vinalia Faculae spectrum (blue line), and Cerealia Facula spectra (red and purple spectra). They are shown after continuum removal. Upper left: absorption band ascribed to ammoniated salts at 2.08, 2.21, 2.34 μm, deeper on Cerealia Facula, and absent from the floor spectrum. Upper right: shift of the band center from 2.72 to 2.76 μm between floor and bright material, ascribed to a changing composition from Mg-phyllosilicates to Al-phyllosilicates. Lower left: ammonium phyllosilicates at 3.06 (black spectrum) in the floor spectrum, and complex spectral region at 3.0 – 3.6 μm, with the superposition of 3.1, 3.2 and 3.28 μm absorption bands, and the absorption band of carbonate at 3.4 and 3.5 μm. Lower right: absorption band of carbonates. The shift from 3.95 μm to 4.01 μm marks the changing composition from Mg-Ca-carbonates to Na-carbonates.

Spectral mapping of the whole crater region is performed by producing a spatial matrix (341 x 341) with a step of 0.05° (~400 m). Taking into account the coordinates of the pixel center of each spectrum, we averaged all derived spectral parameters coming from pixels with the same spatial coordinates, within the step width (Figure 5 shows the redundancy map). All pixels corresponding to an incidence angle > 70°, emission angle > 70°, or in casted shadow have been filtered out to avoid spectral artifacts produced by pixels with low signal to noise ratio (S/N). The information on the viewing geometry and illumination has been calculated from the shape model and the spacecraft position at the time of the observations.
The maps of each spectral feature are discussed in the next subsections.

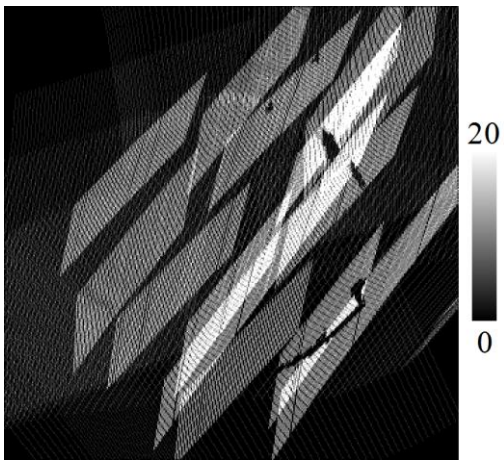

Figure 5. Redundancy map of the matrix which covers the Occator crater region.

4.2 Global maps

Two maps of photometrically corrected reflectance at 2.0 μm with different stretching are shown in Figure 6 in order to point out all the spatial features of the faculae, the floor, and the ejecta. The corrected reflectance represents the I/F as seen in standard viewing geometry (incidence angle =

30°, emission angle = 0°) correcting both for topographic variations and for physical/optical characteristics of the regolith (Ciarniello et al. 2016).
Ceralia Facula, in the center of the crater, is by far the brightest region on the whole Ceres surface. The Vinalia Faculae, composed of two large and several small bright regions, are located in the east part of the floor. Spatial brightness variations can also be detected on the rest of the floor, being brighter near the faculae and in the north-eastern part of the crater rim. Outside the rim, we can notice different types of ejecta as already discussed by Longobardo et al. (submitted). They are particularly darker in the north-eastern part.

The spectral slope map (figure 7) is calculated with a linear fit between 1.65 and 2.35 μm. It represents the angular coefficient divided by the median signal in this spectral range. Different regions can be defined by the spectral slope map: higher values of the slope in the north-eastern ejecta, smaller values corresponding with the faculae. This could be an indication of compositional variations as well as variations in regolith grain size.

Results for the analysis of the 2.7 μm absorption are shown in Figure 8. The dichotomy of the ejecta is visible in its band area: broader in the north-eastern part, and shallower in the western part. Variation of the band area can also be seen in all direction outside the rim with a radial pattern. The bright material of Cerealia Facula shows a shallower band area, indicating a lower concentration of phyllosilicates.
The band center is an indicator of composition: the band centered at 2.76 can indicate mainly Al-phyllosilicates (De Sanctis et al., 2016) and the band centered at 2.72 the presence of Mg-phyllosilicates (De Sanctis et al., 2015). The former mostly matches the bright material, whereas the larger concentration of the latter can be observed at the crater rim.

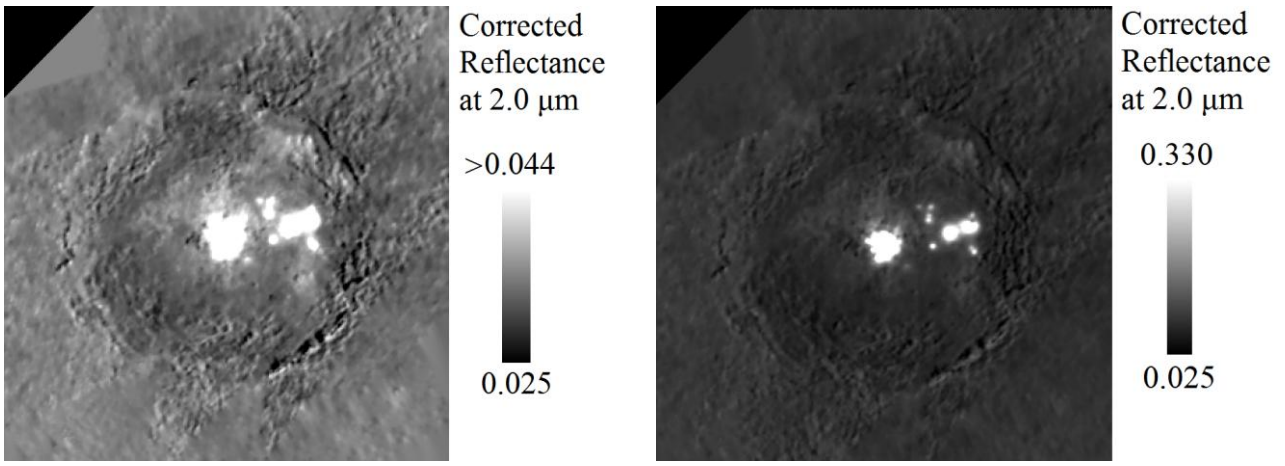

Figure 6. Global maps of photometrically corrected reflectance at 2.0 μm (I/F in standard viewing geometry), with different stretching.

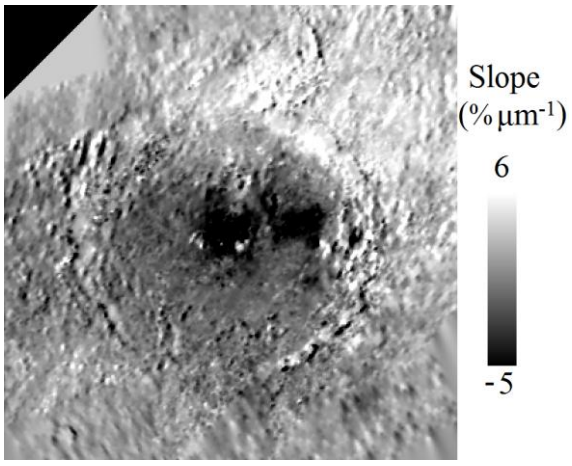

Figure 7. Spectral slope in the range 1.65-2.35 μm.

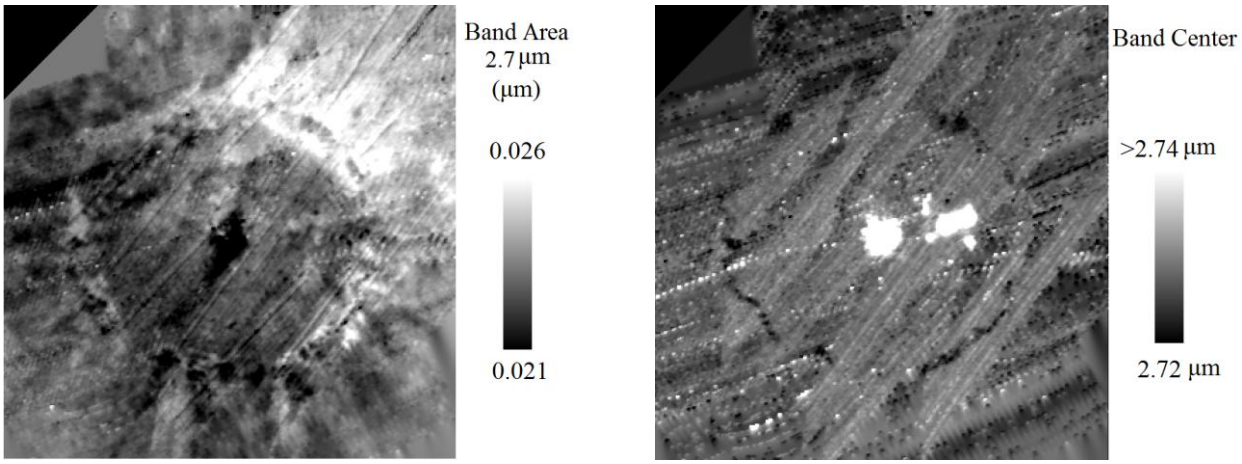

Figure 8. Absorption band at 2.7 μm: band area in the left panel and band center in the right panel. Some stripes are present in the maps as a result of non-filtered artifacts in the spectra.

Carbonate absorption bands at 3.5 and 4.0 μm are well detected once the thermal emission has been removed. Analysis of their band areas reveals a very good correlation with the brightness of the surface material (see Figure 9), with the larger values at the faculae, as already discussed in De Sanctis et al. (2016) (see Figure 10). A good correlation is derived between the band center and the band areas of carbonates absorption bands (right panel of Figure 10), revealing compositional differences between the faculae (mostly Na-carbonates) and the average material (mostly Mg-carbonates). Like in the case of the 2.7-absorption band, relatively larger values of the band area are present at the crater rim.

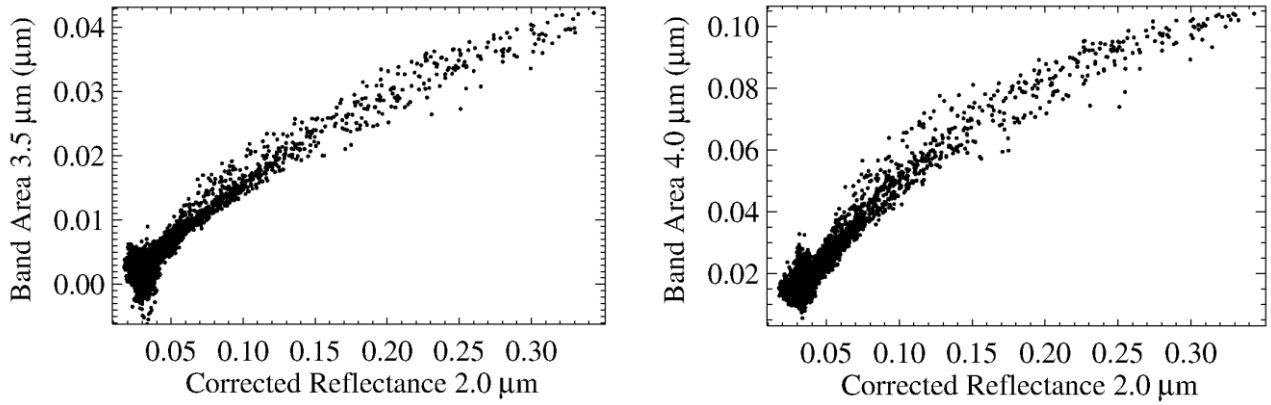

Figure 9. Scatter plot of the carbonate band areas at 3.5 μm (left) and 4.0 μm (right), as a function of the photometrically corrected reflectance at 2.0 μm. Points with higher band area and corrected reflectance are related to the faculae regions.

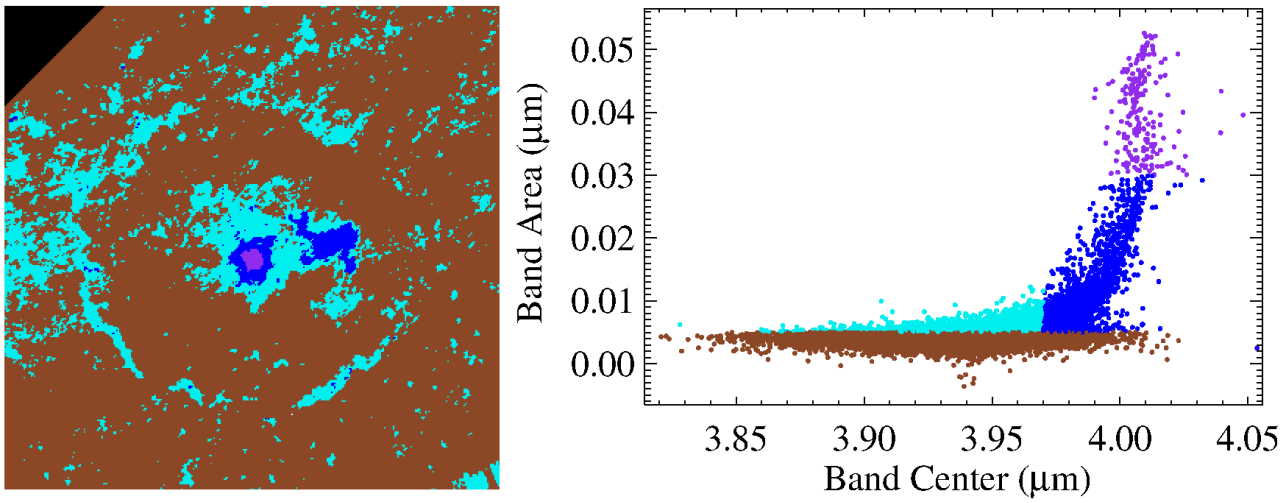

Figure 10. Absorption band center at 4.0 µm as a function of a weighted average of the band areas at 3.5 and 4.0 µm. The colored regions of the map on the left panel match scatter plot colors on the right panel.

The spectral parameters of the 3.1 µm absorption band also reveals a dichotomy in the composition of the ejecta (see figure 11), with larger band area values in the north-eastern part. The scatter plot depicts a "tail" which is related to the bright material of the faculae: smaller band area values and a shift in the band center. This shift still lacks an explanation in term of changing composition. It can be related to different components which are partially mixed in the intermediate regions.

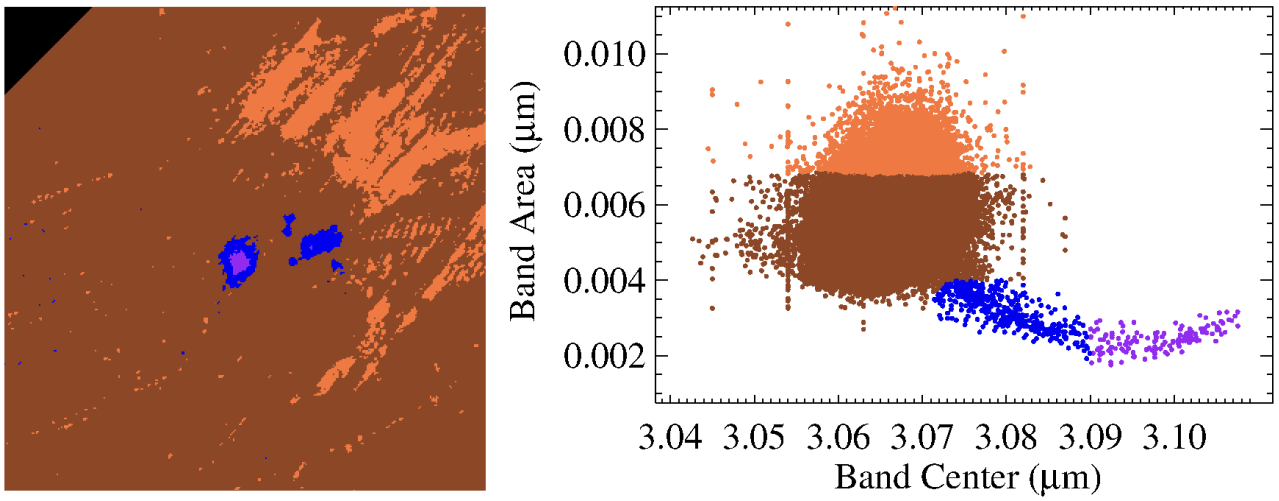

Figure 11. Absorption band center as a function of a band area at 3.1 µm. The colored regions of the map on left panel match the scatter plot colors on the right panel. Two populations of points can be distinguished on the base of density slice analysis; the upper one is related to the ejecta in the north-eastern part of the map and the "tail" of the scatter plot is related to the faculae.

4.3 Faculae compositional maps

The bright material constituting the faculae is analyzed in detail in this subsection.

Figure 12 shows a comparison between well defined spectral parameters of Cerealia Facula: corrected reflectance at 2.0 µm, band area at 4.0 µm, band area at 2.2 µm, and band areas of the two shallower absorption bands at 3.2 and 3.28 µm. There is a very good correlation between carbonate band area and corrected reflectance. This is an indication that carbonates are the main contributor to the photometric properties of the faculae. Good correlation can also be seen for the other two parameters, however significant differences can be noted. This reflects a heterogeneity of the composition. The difference in the band area is also a demonstration that the component(s) responsible for the 3.20 and 3.28 µm absorption bands is different from the minerals producing the other spectral signatures.

As discussed above, the band center of the phyllosilicates absorption band at 2.7 μm is peculiar in the faculae region, and its analysis can well define the edges of the faculae. Figure 13 shows that Cerealia Facula has a very jagged edge, different from the very diffuse edges of the Vinalia faculae.

Further analysis of the 3.20 and 3.28 μm absorptions (figure 14) shows the sum of their band areas as a function of the corrected reflectance at 2.0 μm. The scatter plot reveals that the band areas are correlated to brightness, but with deviations from this trend in specific populations of points: for the same brightness we have smaller band areas in the Vinalia Faculae than in Cerealia Facula, and also significant variations within the Cerealia Facula.

Similar analysis has been performed for the band area at 2.2 μm (see figure 14), which has been ascribed to the presence of ammonium chloride. Also in this case, the scatter plot reveals that the band area is correlated to brightness, but with deviations from this trend in specific populations of points (blue and purple in fig. 14) which present higher band areas. They are related to a region on the facula that presents a peculiar shape, suggesting a distinct formation event.

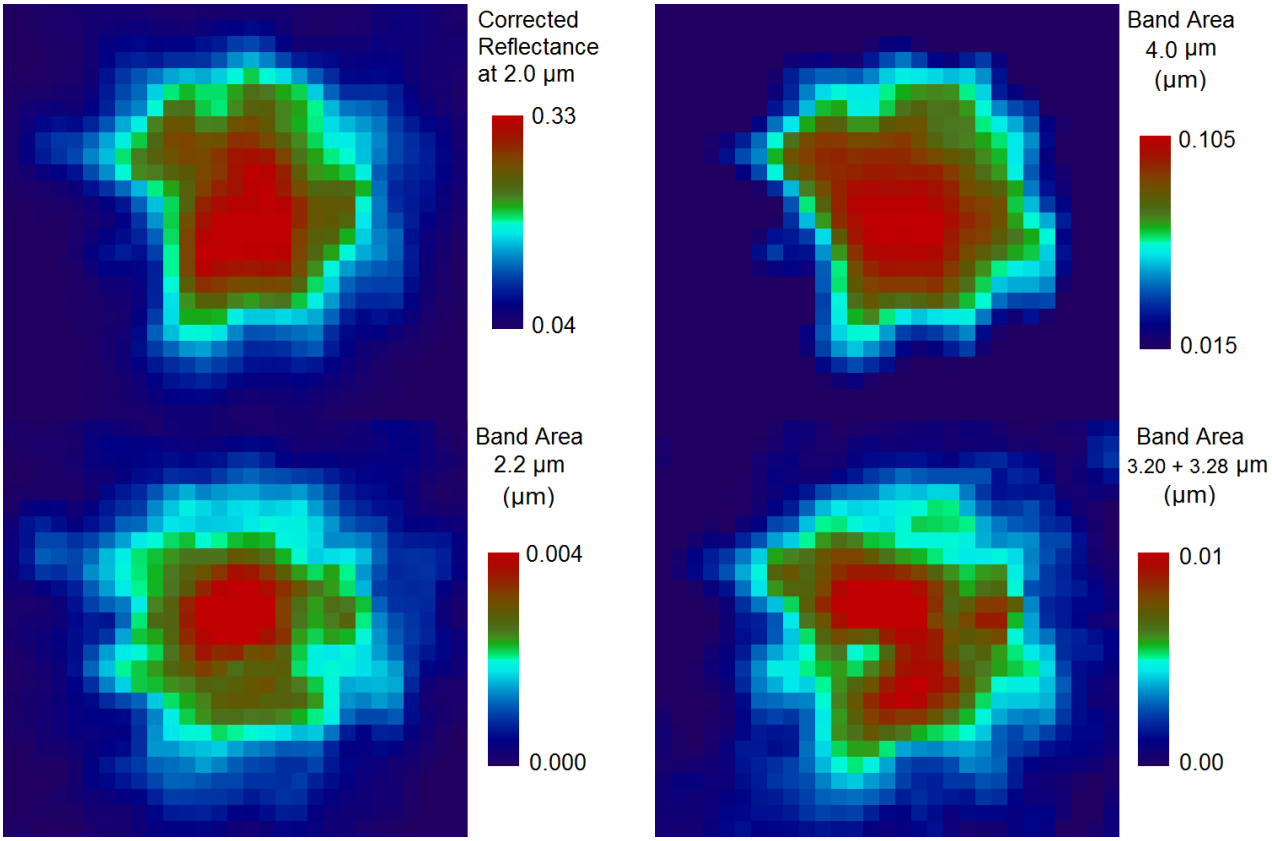

Figure 12. Cerealia Facula maps for different parameters retrieved from the analysis described in Section 4.

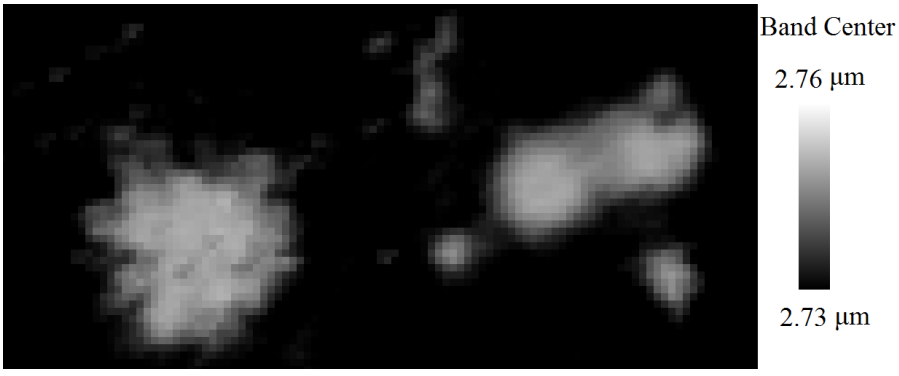

Figure 13. Center of the 2.7 μm absorption band mapped to the faculae.

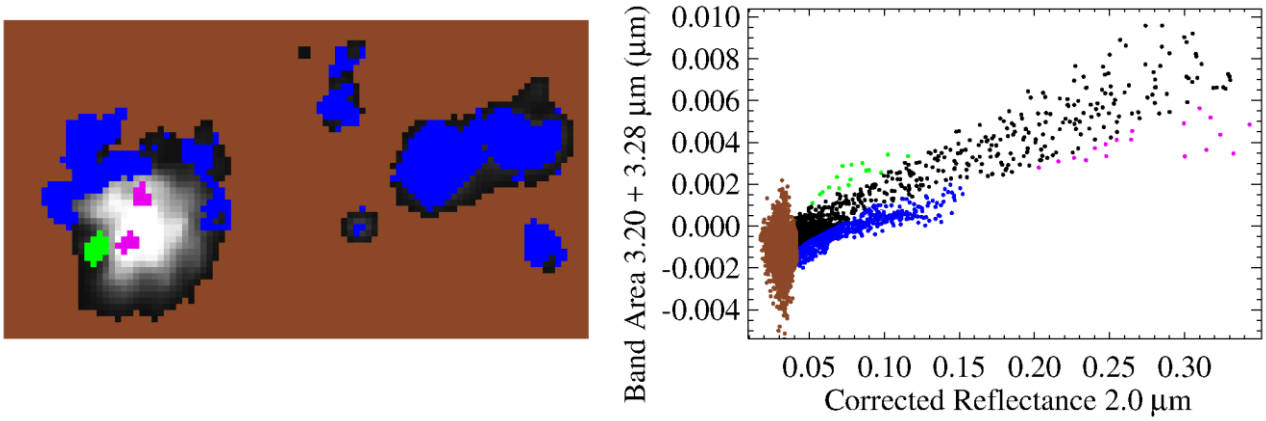

Figure 14. Areas of absorption bands at 3.20 and 3.28 µm as a function of the corrected reflectance at 2.0 µm. Different populations of points are divided on the base of their deviation from the general trend and on the base of the density slice analysis. Purple regions correspond to the purple spectrum in figures 3 and 4.

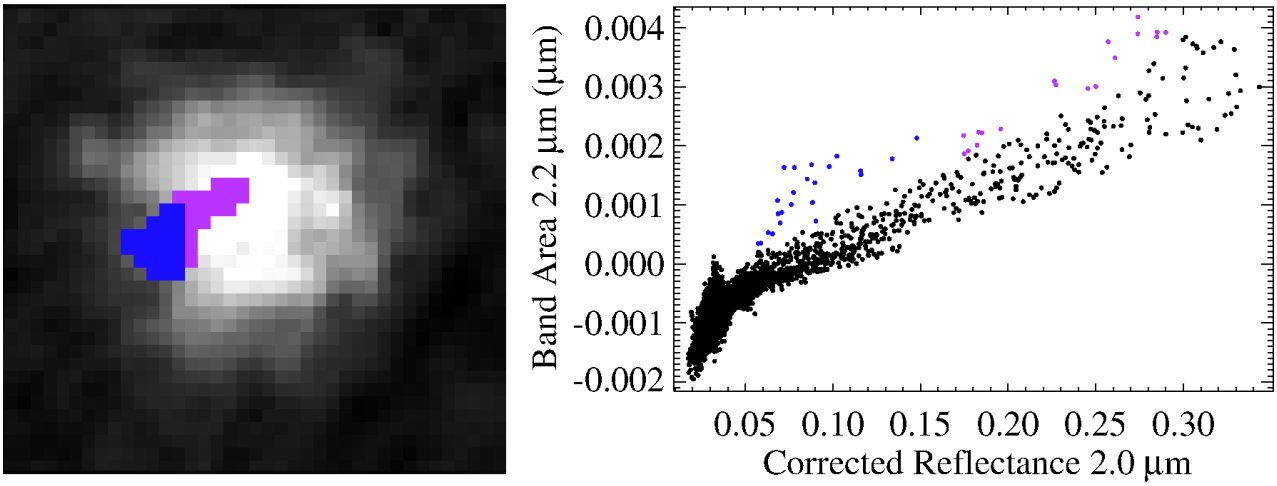

Figure 15. Area of the absorption band at 2.2 µm as a function of the corrected reflectance at 2.0 µm. Blue points clearly belong to a distinct population. Here we also highlight the purple region characterized by broader band area than the average trend, which possibly shares a common origin with the blue region in term of evolution of the facula. The blue region is partially overlapped by the green region of Figure 14.

5. Spectral Modeling

To obtain an information on the abundances of the minerals making up the surface, we used a quantitative spectral analysis of the composition using Hapke's radiative transfer model (Hapke 1993, 2012) as described by Ciarniello et al. (2011) and Raponi et al. (2016). The whole formulation of the bidirectional reflectance (r) is:

Eq. 1 $$r = \frac{SSA}{4\pi}\frac{\mu_0}{\mu+\mu_0}\left[B_{SH}p(g) + H(SSA,\mu)H(SSA,\mu_0) - 1\right] \times S(i,e,g,\theta)\, B_{CB}$$

Where i, e, g are the incidence, emission, and phase angles, respectively, and μ_0, μ are the cosines of the incidence and emission angles. These parameters come from the shape model and position of the spacecraft at the time of observation. The parameters that contain most of the spectral information are the single scattering albedo (*SSA*), and the related Ambartsumian–Chandrasekhar functions $H(SSA, \mu)$ describing the multiple scattering components.

Other parameters describe the photometric behavior as a function of the viewing geometry, especially the phase function; they are:

- the single particle phase function $p(g)$,
- the shadow hiding opposition effect $B_{SH}(g)$,

- the coherent back-scattering opposition effect $B_{CB}(g)$,
- the shadow function modelling large-scale roughness $S(i, e, g, \theta)$, with θ being the average surface slope.

These photometric parameters are fixed after Ciarniello et al. (2015), who defined the average scattering properties of Ceres' regolith. We assume their values are equal in all types of terrains considered in this work (ejecta, floor, faculae). This assumption is endorsed by the work of Longobardo et al. (this issue) which obtained very similar phase functions for the different terrains.
The spectral properties are mainly affected by the SSA parameters. The latter have been modeled for an intimate mixing between different minerals, which implies that the particles of the end-member materials are in contact with each other and all are involved in the scattering of a single photon. The SSA of each mineral is defined starting from their grain size and their optical constants as described in Hapke (2012). The optical constants are derived from laboratory measurements (Table 1) with the method described by Carli et al. (2014).
The average SSA of the regolith is defined through the weights p, which represent the relative abundances of the minerals. The weight p_i is defined as the cross section of the grains of the *ith* mineral as a fraction of the area. p is also a volume fraction, assuming grain sizes are equal for all minerals. Hereafter we refer to the weights p as "abundances".

Eq. 2 $$SSA = SSA_1 p_1 + SSA_2 p_2 + SSA_3 p_3 + .. \quad \text{with: } p_1 + p_2 + p_3 + .. = 1$$

The best-fitting result is obtained by comparison of the model with the measured spectra, applying the Levenberg–Marquardt method for non-linear least-squares multiple regression (Marquardt 1963) (see Figure 16).
Free model parameters to be retrieved are:
(i) abundances of the end-members and their grain sizes (assumed equal for all end-members);
(ii) a multiplicative constant of the absolute level of reflectance of the model in order to account for uncertainties in the radiometric and photometric accuracies, as well as errors on the local geometry information due to unresolved shadows and roughness;
(iii) a slope added to the model in order to better fit the measured spectrum: in some cases, the measured spectra present an artificial slope where high signal contrast is measured between adjacent pixels, like regions near shadows. This is due to a varying spatial point spread function towards longer wavelengths (Filacchione 2006);
(iv) temperature and effective emissivity (Davidsson et al., 2009). The latter is the product of the directional emissivity (Hapke 2012) and a free parameter used to account for unresolved shadow and the structure of the surface (Davidsson et al. 2009). Its interpretation is outside the scope of this work.
The total radiance is modeled by accounting for both the contributions of the reflected sunlight, and the thermal emission:

Eq. 3 $$Rad = r \times \frac{F_\odot}{D^2} + \varepsilon_{eff} \times B(\lambda, T)$$

where r is the Hapke bidirectional reflectance (Eq.1), $F_\odot$ is the solar irradiance at 1 AU, D is the heliocentric distance (in AU), ε_{eff} is the effective emissivity, $B(\lambda, T)$ is the Planck function. Thus, the estimation of the thermal emission discussed in Section 3 is done simultaneously with the reflectance modeling in order to yield a consistent result between these two contributions to the total signal measured.
The SSA is modeled starting from minerals already discussed in De Sanctis et al. (2015, 2016) (see Table 1) which are related to the average Ceres surface and the composition of the Faculae.

Mineral	Type	Sample ID
Antigorite	Mg-phyllosilicate	AT-TXH-007
Dolomite	Mg-Ca-carbonate	CB-EAC-003
NH_4-montmorillonite	NH_4-phyllosilicate	JB-JLB-189
Magnetite	Dark material	MG-EAC-002
Heated Natrite	Na-carbonate	CB-EAC-034-C
Natrite (+H_2O)	Na-carbonate	CB-EAC-034-A
Illite	Al-phyllosilicate	IL-EAC-001
Ammonium Chloride	NH_4-salt	CL-EAC-049-A
Ammonium Bicarbonate	NH_4-carbonate	CB-EAC-041-B

Table 1. End-members used in calculating optical constants of the mineral types. Spectra are taken from the Relab spectral database.

In our previous analysis, this band was assigned to ammonium bicarbonate or ammonium chloride, due to the difficulty in determining unambiguously the carrier. Here, thanks to the high spatial resolution data taken during LAMO orbit the absorption band at 2.2 μm is detected with a high S/N, establishing the role of ammonium chloride in producing this band. Thus, we rule out the ammonium bicarbonate that has been previously considered by De Sanctis et al. (2016) (see figure 17) as a possible component of the mixture. However, a volume amount lower than 1% of ammonium bicarbonate is still possible because smaller than the detection limit.

Optical constants of sodium carbonates have been derived from two measured spectra of the same sample under different conditions: hydrated and anhydrous (Carrozzo et al. 2017). When optical constants from both spectra are taken into account, we obtain marginally better fits. However, we cannot establish the presence of hydrated sodium carbonate in the faculae, because the signature of hydration, if present, is shallower than the detection limit.

The maps of abundances (Figure 18) and grain size (Figure 19) are superimposed to the Framing Camera mosaic with a transparency of 25% in order to highlight the morphological context.
Sodium carbonate is the most abundant component of the faculae. In the rest of Ceres' surface the predominant component is a dark material, whose identification is challenging, because its spectrum is featureless, except for the tentative absorption band centered at 1 μm, which can be attributed to iron (Fe). We found a good fit with magnetite (Fe_3O_4), however, a large amount of Fe is not consistent GRAND measurements (Prettyman et al. 2017). More likely dark surface of Ceres should be composed by a large amount of carbon bearing material, being carbonaceous chondrite its close meteoritic analogue (Chapman, C. R. & Salisbury, J. W., 1973, McSween et al., 2017). Moreover, we emphasize that the model used in this work is only based on spectral features, being the absolute signal level of the model adjusted with the multiplicative constant and the additional slope (fig. 20).
The map of grain size (Figure 19) shows differences among north-estern ejecta (30-60 μm), average crater floor (100-130 μm), peripheral material of the facuale (100-130 μm), central material of the faculae (10-60 μm). The average regolith outside the crater has a grain size of ~100 μm.

Not all measured spectra have been well modeled. In particular, the faculae spectra present some features that are still unexplained in term of composition (see Figure 16), such as the absorption bands at 3.10, 3.20, and 3.28 μm.

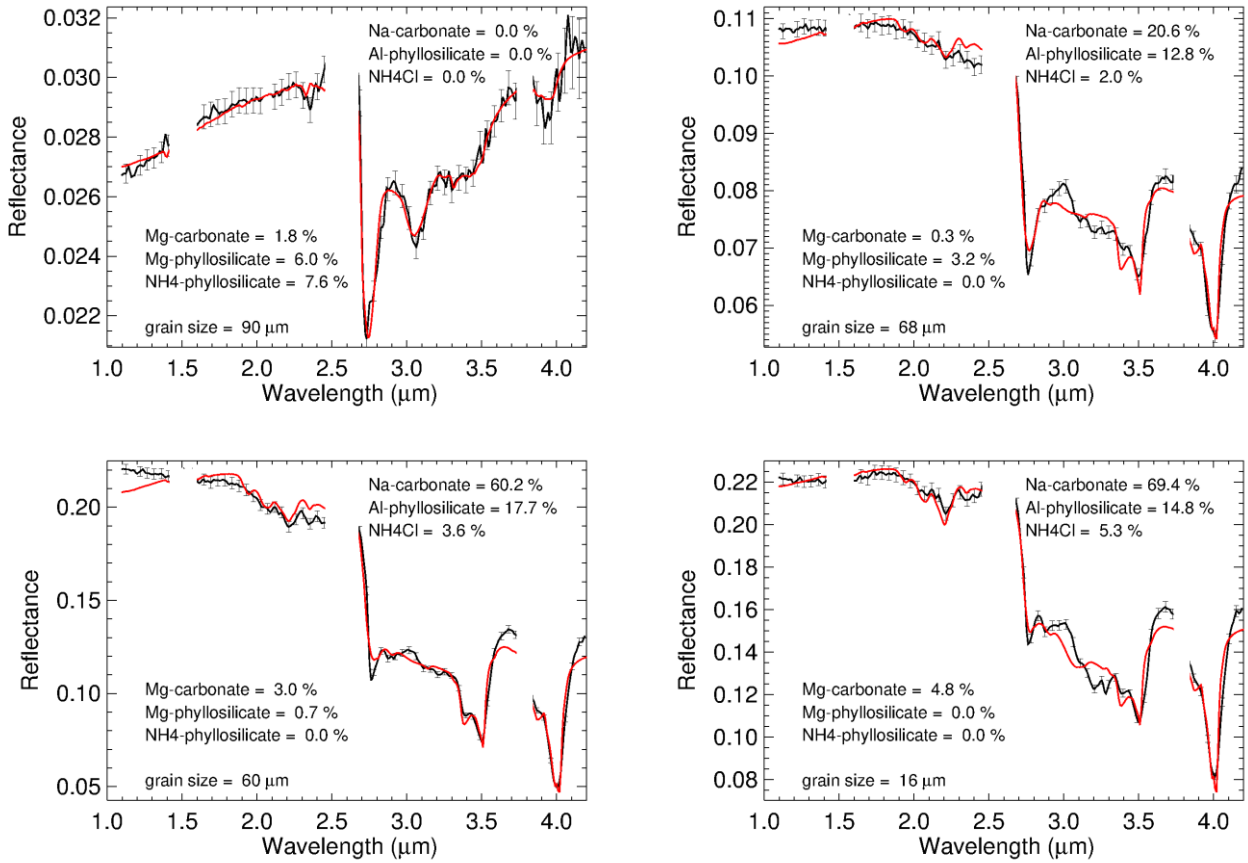

Figure 16. Four examples of best fit of measured spectra: crater ejecta (upper left), Vinalia Faculae (upper right), and two spectra of Cerealia Facula. Error bars include poissonian noise and calibration uncertainties.

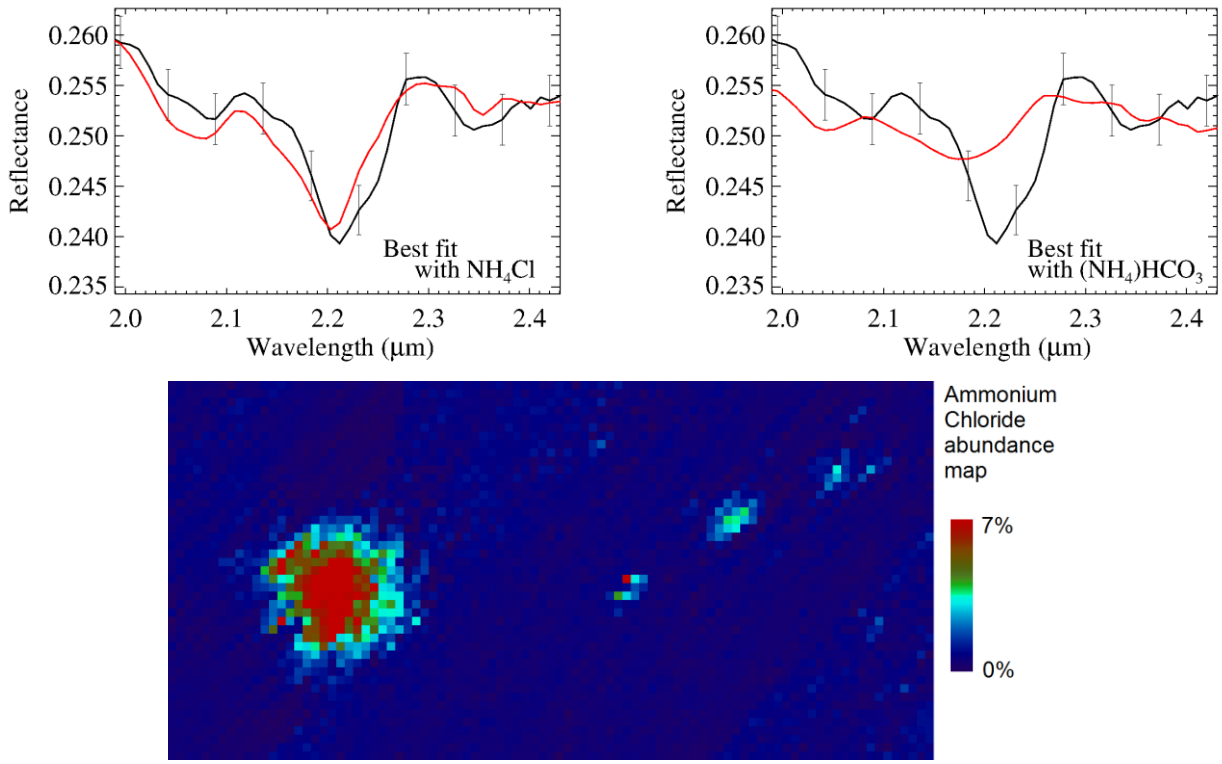

Figure 17. Upper panels: Measured absorption band at 2.2 µm on Cerealia Facula (black line), and model (red line) performed with ammonium chloride (upper left), and ammonium carbonate (upper right). Bottom panel: abundance map of ammonium chloride. The modeling indicates the presence of this mineral on the rest of Occator crater is negligible.

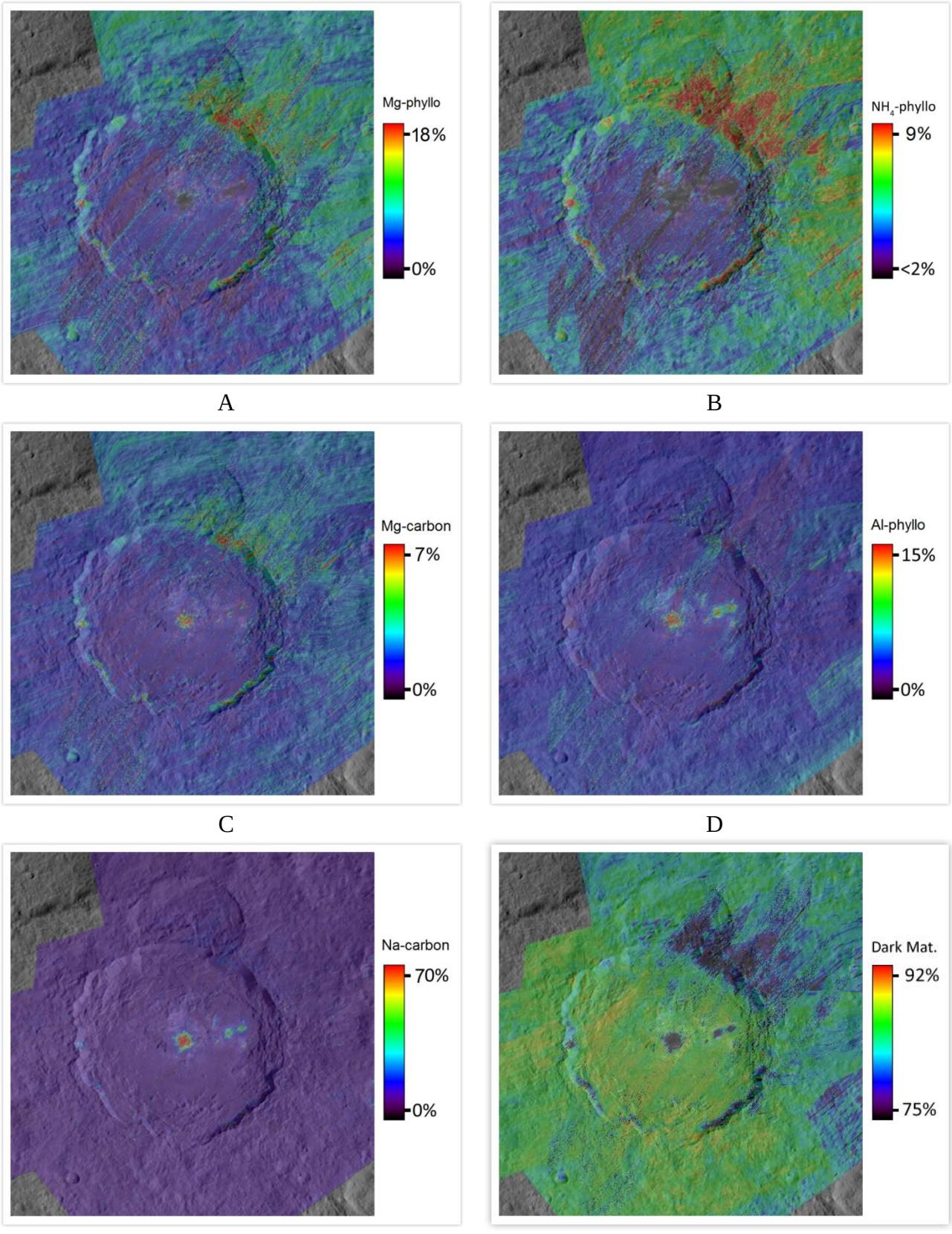

Figure 18. Abundance maps of: A: Mg-phyllosilicate B: NH_4-phyllosilicate. C: Mg-carbonate. D: Al-phyllosilicate. E: Na-carbonate. F: Dark material.

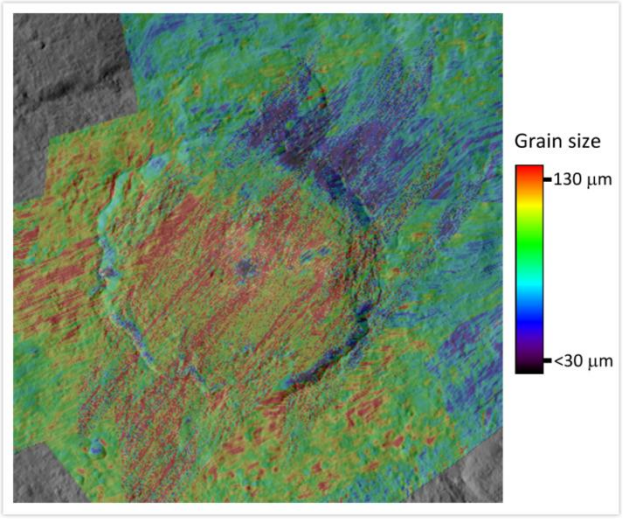

Figure 19. Grain diameter map.

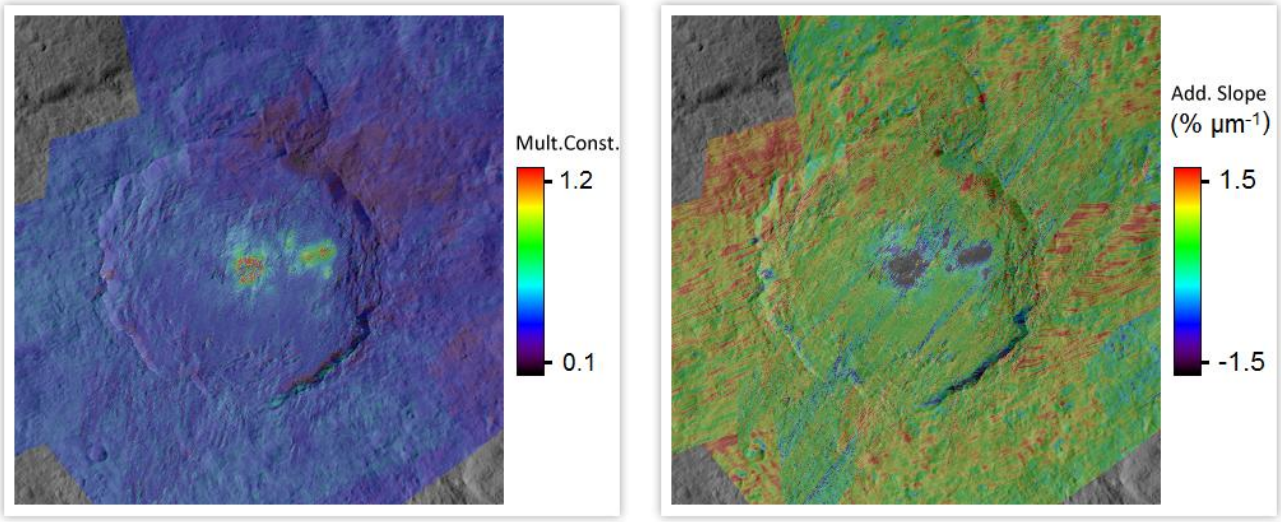

A B

Figure 20. Multiplicative constant (A) and additional slope (B) maps.

6. Discussion and Conclusions

The region of Occator crater presents a very diversified mineralogy. Each part of the crater (ejecta, floor, faculae) could reveal insights about formation and evolution of the dwarf planet. From spectral analysis and spectral modeling, we detect very peculiar ejecta in the north-eastern part of the crater, which shows a larger abundance of all components present on the average surface of Ceres (Mg-phyllosilicates, Mg-Carbonates, NH_4-phyllosilicates), and thus a smaller modeled amount of dark material. These detections are apparently in contradiction with the lower albedo of that ejecta, which is in fact compensated in the model with a lower multiplicative constant. This apparent contradiction of the model can be solved by assuming at least two different types of dark materials: the dark ejecta has a lower concentration of dark material than the rest of the surface but is dominated by a different type of dark material of much lower albedo.

The grain size is also peculiar in these ejecta: the small grain size retrieved for the bright material suggests the rapid cooling of this material following emplacement onto the surface.

Very similar parameters have been derived for the ejecta and crater walls. This points to a common origin in a reservoir that was lately spread on the surface by the Occator impact event, mostly on the ejecta and partially on the crater walls. Differences of the content of phyllosilicates and carbonates on the global surface of Ceres have already been discussed by Ammannito et al. (2016) and Carrozzo et al. (2017). These differences could be primordial, or reveal a heterogeneous convective-

like process with upwelling of subsurface material. In both cases the material has experienced lateral mixing by micrometeoritic impacts. The peculiar ejecta in the north-eastern part of the Occator crater would be an example of this reservoir of material slightly different from the rest of the surface, and preexistent to the impact event of the Occator crater.

The spectral analysis of the floor near the faculae reveals material which has intermediate properties between bright material and average regolith, pointing to bright material deposition events older than the faculae formation, partially buried by lateral mixing. This is confirmed by the morphological analysis of the crater floor (Scully et al. this issue). The northeastern part of the floor, in which bright material is present, is likely temporally linked to these older deposition events. However, a significant difference with respect the faculae material is represented by the larger grain size in all the crater floor. The larger grain size would point to slower cooling condition, in which larger grains can grow, for example in a melt reservoir. Contrarily, a fast cooling should have taken for the bright material of the faculae, especially in the center of Cerealia Facula, in correspondence of the reddish dome (Figure 1). For this reason, the deposition event of floor material could have been very close to the impact event, unlike the more recent faculae formations.

The significant depletion of NH_4-phyllosilicates, and the slight depletion of Mg-phyllosilicates on the floor of the crater are quite common on other Ceres craters (e.g. Ammanito et al., 2016, Longobardo et al. submitted, De Sanctis et al., submitted, Raponi et al. submitted), and could be related to the release of NH_4^+ and OH^- as a consequence of impact induced heating.

The specific analysis performed for the faculae has highlighted differences between the Cerealia and Vinalia areas for both mineralogy and morphology. The composition of the Vinalia Faculae present a lower concentration of all components that are present on Cerealia facula: Na-carbonate, NH_4Cl, Al-phyllosilicates, and the unknown component(s) responsible for the bands at 3.20 and 3.28 μm. Moreover, from the map of the band center at 2.7 μm we also find different shapes for the facula edges: jagged for Cerealia Facula and smooth for Vinalia Faculae.
These differences may have several explanations: i) different kind of emplacements (Zolotov 2017), ii) different stages of the formation mechanism, iii) different intensities of the formation mechanism (Ruesch et al. 2017), iv) different epochs of formation: the lateral mixing from micrometeoritic impacts partially buried the oldest bright material.

Notable differences in the mineralogy are also observed across Cerealia Facula. The mineral distribution does not seem homogeneous and it is not perfectly correlated to the brightness of the surface, revealing peculiar regions inside the Facula. From the band area map of the ammonium chloride in Cerealia Facula, we identified a region with higher concentration than the average trend, whose shape suggests a different deposition event. Partial superposition between this region and an excess of band area at 3.20 and 3.28 μm can be also noted.

The spectral modeling performed in this work made use of the well established components of the average surface and faculae materials. We also established the role of the ammonium chloride in producing the absorption band at 2.2 μm. However, some aspects Ceres' composition remain unexplained. In particular, the surface darkening agent is featureless and thus unrecognizable. Moreover, more than one type of dark material should be present based on the above discussion on the nature of the ejecta. We also miss at least one component of the faculae material, which is/are responsible for the absorption bands at 3.11, 3.20 and 3.28 μm. The missing component(s) is/are probably different from the other minerals on the faculae, on the basis of the spectral modeling and of the monitoring of band area distributions. The need for a multiplicative constant and additional slope with systematically different values on the faculae with respect to the rest of Ceres surface can be explained by the fact that those missing materials alter the signal level in a way that cannot be modeled from the minerals taken into account. Thus the additional parameters have to compensate for them to match the signal level. Further effort with extracting information from the Dawn

datasets should be made to complete the mineralogy of Ceres average surface and the faculae, which could reveal more about the evolution of the dwarf planet.

Acknowledgments
VIR is funded by the Italian Space Agency-ASI and was developed under the leadership of INAF-Istituto di Astrofisica e Planetologia Spaziali, Rome-Italy. The instrument was built by Selex-Galileo, Florence-Italy. The authors acknowledge the support of the Dawn Science, Instrument, and Operations Teams. This work was supported by ASI and NASA.

References

Ammannito, E., De Sanctis, M.C., Ciarniello, M., Frigeri, A., Carrozzo, F.G., Combe, J.-Ph., Ehlmann, B.L., Marchi, S., McSween, H.Y., Raponi, A., Toplis, M.J., Tosi, F., Castillo-Rogez, J.C., Capaccioni, F., Capria, M.T., Fonte, S., Giardino, M., Jaumann, R., Longobardo, A., Joy, S.P., Magni, G., McCord, T.B., McFadden, L.A., Palomba, E., Pieters, C.M., Polanskey, C.A., Rayman, M.D., Raymond, C.A., Schenk, P.M., Zambon, F., Russell, C.T., 2016. Distribution of phyllosilicates on the surface of Ceres. Science 353 (6303), id.aaf4279. Doi: 10.1126/science.aaf4279.

Buczkowski, D. L.; Schmidt, B. E.; Williams, D. A.; Mest, S. C.; Scully, J. E. C.; Ermakov, A. I.; Preusker, F.; Schenk, P.; Otto, K. A.; Hiesinger, H.; O'Brien, D.; Marchi, S.; Sizemore, H.; Hughson, K.; Chilton, H.; Bland, M.; Byrne, S.; Schorghofer, N.; Platz, T.; Jaumann, R.; Roatsch, T.; Sykes, M. V.; Nathues, A.; De Sanctis, M. C.; Raymond, C. A.; Russell, C. T. The geomorphology of Ceres. Science, 353, id.aaf4332 (2016).

Carli, C.; Ciarniello, M.; Capaccioni, F.; Serventi, G.; Sgavetti, M. Spectral variability of plagioclase-mafic mixtures (2): Investigation of the optical constant and retrieved mineral abundance dependence on particle size distribution. Icarus, 235, p. 207-219 (2014).

Carrozzo, F.G., Raponi, A., De Sanctis, M.C., Ammannito, E., Giardino, M., D'Aversa, E., Fonte, S., Tosi, F., 2016. Artifacts reduction in VIR/Dawn data. Rev. Sci. Instrum. 87 (12), id.124501. Doi: 10.1063/1.4972256.

Carrozzo, F.G., De Sanctis, M.C., Raponi, A., Ammannito, E., Castillo-Rogez, J.C., Ehlmann, B.L., Marchi, S., Stein, N., Ciarniello, M., Tosi, F., Capaccioni, F., Capria, M.T., Fonte, S., Formisano, M., Frigeri, A., Giardino, M., Longobardo, A., Magni, G., Palomba, E., Zambon, F., Raymond, C.A., Russell, C.T., 2017a. Nature, formation and distribution of Carbonates on Ceres. Submitted to Science Advances. Under review.

Chapman, C. R. & Salisbury, J. W. Comparisons of meteorite and asteroid spectral reflectivities. Icarus 19, 507–522 (1973).

Ciarniello, M.; Capaccioni, F.; Filacchione, G.; Clark, R. N.; Cruikshank, D. P.; Cerroni, P.; Coradini, A.; Brown, R. H.; Buratti, B. J.; Tosi, F.; Stephan, K. Hapke modeling of Rhea surface properties through Cassini-VIMS spectra. Icarus, 214, p. 541-555 (2011).

Ciarniello, M., De Sanctis, M.C., Ammannito, E., Raponi, A., Longobardo, A., Palomba, E., Carrozzo, F.G., Tosi, F., Li, J.-Y., Schröder, S.E., Zambon, F., Frigeri, A., Fonte, S., Giardino, M., Pieters, C.M., Raymond, C.A., Russell, C.T., 2017. Spectrophotometric properties of dwarf planet Ceres from the VIR spectrometer on board the Dawn mission. Astron. Astrophys. 598, id.A130. Doi: 10.1051/0004-6361/201629490.

Davidsson, Björn J. R.; Gutiérrez, Pedro J.; Rickman, Hans. Physical properties of morphological units on Comet 9P/Tempel 1 derived from near-IR Deep Impact spectra. Icarus, 201, p. 335-357 (2009).

De Sanctis, M.C., Coradini, A., Ammannito, E., Filacchione, G., Capria, M.T., Fonte, S., Magni, G., Barbis, A., Bini, A., Dami, M., Ficai-Veltroni, I., Preti, G., and the VIR Team, 2011. The VIR Spectrometer. Space Sci Rev. 163, Issue 1–4, 329-369. Doi: 10.1007/s11214-010-9668-5.

De Sanctis, M.C., Ammannito, E., Raponi, A., Marchi, S., McCord, T.B., McSween, H.Y., Capaccioni, F., Capria, M.T., Carrozzo, F.G., Ciarniello, M., Longobardo, A., Tosi, F., Fonte, S., Formisano, M., Frigeri, A., Giardino, M., Magni, G., Palomba, E., Turrini, D., Zambon, F., Combe, J.-Ph., Feldman, W., Jaumann, R.,

McFadden, L.A., Pieters, C.M., Prettyman, T., Toplis, M., Raymond, C.A., Russell, C.T., 2015. Ammoniated phyllosilicates with a likely outer Solar System origin on (1) Ceres. Nature 528 (7581), 241-244. Doi: 10.1038/nature16172.

De Sanctis, M.C., Raponi, A., Ammannito, E., Ciarniello, M., Toplis, M.J., McSween, H.Y., Castillo-Rogez, J.C., Ehlmann, B.L., Carrozzo, F.G., Marchi, S., Tosi, F., Zambon, F., Capaccioni, F., Capria, M.T., Fonte, S., Formisano, M., Frigeri, A., Giardino, M., Longobardo, A., Magni, G., Palomba, E., McFadden, L.A., Pieters, C.M., Jaumann, R., Schenk, P., Mugnuolo, R., Raymond, C.A., Russell, C.T., 2016. Bright carbonate deposits as evidence of aqueous alteration on (1) Ceres. Nature 536 (7614), 54-57. Doi: 10.1038/nature18290.

Filacchione, Gianrico. Calibrazioni a terra e prestazioni in volo di spettrometri ad immagine nel visibile e nel vicino infrarosso per l'esplorazione planetaria. Ph.D thesis, Università di Napoli Federico II, 316 pages, 2006.

Filacchione, G., and Ammannito, E., 2014. Dawn VIR calibration document. version 2.4, http://sbn.psi.edu/archive/dawn/vir/dwnvvir_i1b/document/vir_calibration/vir_calibration_v2_4.pdf.

Hapke B., Theory of reflectance and emittance spectroscopy, 1993.

Hapke B., 1993, Theory of reflectance and emittance spectroscopy Second Edition, 2012

Konopliv, A. S.; Asmar, S. W.; Bills, B. G.; Mastrodemos, N.; Park, R. S.; Raymond, C. A.; Smith, D. E.; Zuber, M. T. The Dawn Gravity Investigation at Vesta and Ceres. Space Science Reviews, 163, pp. 461-486

Li, Jian-Yang; Reddy, Vishnu; Nathues, Andreas; Le Corre, Lucille; Izawa, Matthew R. M.; Cloutis, Edward A.; Sykes, Mark V.; Carsenty, Uri; Castillo-Rogez, Julie C.; Hoffmann, Martin; Jaumann, Ralf; Krohn, Katrin; Mottola, Stefano; Prettyman, Thomas H.; Schaefer, Michael; Schenk, Paul; Schröder, Stefan E.; Williams, David A.; Smith, David E.; Zuber, Maria T.; Konopliv, Alexander S.; Park, Ryan S.; Raymond, Carol A.; Russell, Christopher T. Surface Albedo and Spectral Variability of Ceres. The Astrophysical Journal Letters, 817, article id. L22, 7 pp. (2016).

Longobardo, A., et al., 2017. Mineralogy of the Occator quadrangle. Submitted to Icarus. Under review.

Longobardo A. et al. this issue.

Marquardt D., 1963, SIAM J. Appl. Math., 11, 431

Nathues, A.; Platz, T.; Thangjam, G.; Hoffmann, M.; Mengel, K.; Cloutis, E. A.; Le Corre, L.; Reddy, V.; Kallisch, J.; Crown, D. A. Evolution of Occator Crater on (1) Ceres. The Astronomical Journal, 153, article id. 112, 12 pp. (2017).

Palomba E. et al. this issue.

Prettyman, Thomas H.; Feldman, William C.; McSween, Harry Y.; Dingler, Robert D.; Enemark, Donald C.; Patrick, Douglas E.; Storms, Steven A.; Hendricks, John S.; Morgenthaler, Jeffery P.; Pitman, Karly M.; Reedy, Robert C. Dawn's Gamma Ray and Neutron Detector. Space Science Reviews, 163, pp. 371-459 (2011)

Prettyman, T. H.; Yamashita, N.; Toplis, M. J.; McSween, H. Y.; Schörghofer, N.; Marchi, S.; Feldman, W. C.; Castillo-Rogez, J.; Forni, O.; Lawrence, D. J.; Ammannito, E.; Ehlmann, B. L.; Sizemore, H. G.; Joy, S. P.; Polanskey, C. A.; Rayman, M. D.; Raymond, C. A.; Russell, C. T. Extensive water ice within Ceres' aqueously altered regolith: Evidence from nuclear spectroscopy. Science, 355, pp. 55-59 (2017).

Raponi, A.; Ciarniello, M.; Capaccioni, F.; Filacchione, G.; Tosi, F.; De Sanctis, M. C.; Capria, M. T.; Barucci, M. A.; Longobardo, A.; Palomba, E.; Kappel, D.; Arnold, G.; Mottola, S.; Rousseau, B.; Rinaldi, G.; Erard, S.; Bockelee-Morvan, D.; Leyrat, C. The temporal evolution of exposed water ice-rich areas on the surface of 67P/Churyumov–Gerasimenko: spectral analysis. MNRAS 462, 2016.

Raponi, A., et al., 2017. Mineralogy of the Coniraya quadrangle. Submitted to Icarus. Under review.

Roatsch, T., Kersten, E., Matz, K.-D., Preusker, F., Scholten, F., Jaumann, R., Raymond, C.A., Russell, C.T.,

2016a. Ceres survey atlas derived from Dawn Framing Camera images. Planet. Space Sci. 121, 115-120. Doi: 10.1016/j.pss.2015.12.005.

Roatsch, T., Kersten, E., Matz, K.-D., Preusker, F., Scholten, F., Jaumann, R., Raymond, C.A., Russell, C.T., 2016b. High-resolution Ceres High Altitude Mapping Orbit atlas derived from Dawn Framing Camera images. Planet. Space Sci. 129, 103-107. Doi: 10.1016/j.pss.2016.05.011.

Ruesch, O.; Nathues, A.; Jaumann, R.; Quick, L. C.; Bland, M. T.; Bowling, T. J.; Byrne, S.; Castillo-Rogez, J. C.; Hiesinger, H.; Krohn, K.; McFadden, L. A.; Neesemann, A.; Otto, K.; Schenk, P.; Scully, J.; Sykes, M. V.; Williams, D. A.; Raymond, C. A.; Russell, C. T. Faculae on Ceres: Possible Formation Mechanisms. 48th Lunar and Planetary Science Conference, held 20-24 March 2017, at The Woodlands, Texas. LPI Contribution No. 1964, id.2435 (2017).

Russell, C. T.; Raymond, C. A. The Dawn Mission to Vesta and Ceres. Space Science Reviews, 163, pp. 3-23, 2011.

Schröder, S. E.; Mottola, S.; Carsenty, U.; Ciarniello, M.; Jaumann, R.; Li, J.-Y.; Longobardo, A.; Palmer, E.; Pieters, C.; Preusker, F.; Raymond, C. A.; Russell, C. T. Resolved spectrophotometric properties of the Ceres surface from Dawn Framing Camera images. Icarus, Volume 288, p. 201-225 (2017).

Scully J. et al. this issue.

Sierks, H., Keller, H.U., Jaumann, R., Michalik, H., Behnke, T., Bubenhagen, F., Büttner, I., Carsenty, U., Christensen, U. Enge, R., Fiethe, B., Gutiérrez-Marqués, P., Hartwig, H., Krüger, H., Kühne, W., Maue, T., Mottola, S., Nathues, A., Reiche, K.-U., Richards, M.L., Roatsch, T., Schröder, S.E., Szemerey, I., Tschentscher, M., 2011. The Dawn Framing Camera. Space Sci Rev. 163, Issue 1–4, 263-327. Doi: 10.1007/s11214-011-9745-4.

Stein N. et al. this issue.